ASTROCHEMISTRY

Detection of two interstellar polycyclic aromatic hydrocarbons via spectral matched filtering

Brett A. McGuire[1,2,3]*, Ryan A. Loomis[2]†, Andrew M. Burkhardt[3]†, Kin Long Kelvin Lee[1,3], Christopher N. Shingledecker[4,5,6], Steven B. Charnley[7], Ilsa R. Cooke[8], Martin A. Cordiner[7,9], Eric Herbst[10,11], Sergei Kalenskii[12], Mark A. Siebert[11], Eric R. Willis[10], Ci Xue[10], Anthony J. Remijan[2], Michael C. McCarthy[3]

Unidentified infrared emission bands are ubiquitous in many astronomical sources. These bands are widely, if not unanimously, attributed to collective emissions from polycyclic aromatic hydrocarbon (PAH) molecules, yet no single species of this class has been identified in space. Using spectral matched filtering of radio data from the Green Bank Telescope, we detected two nitrile-group–functionalized PAHs, 1- and 2-cyanonaphthalene, in the interstellar medium. Both bicyclic ring molecules were observed in the TMC-1 molecular cloud. In this paper, we discuss potential in situ gas-phase PAH formation pathways from smaller organic precursor molecules.

Aromatic molecules are a ubiquitous structural motif in organic chemistry and the chemical evolution of the Universe. Of all interstellar carbon, 10 to 25% is thought to be incorporated into polycyclic aromatic hydrocarbons (PAHs), which are expected to form primarily (if not exclusively) in the circumstellar envelopes of evolved stars (*1*). The aromatic molecule benzonitrile (BN; *c*-C_6H_5CN) has been detected in TMC-1, located within the interstellar Taurus Molecular Cloud (*2*), far from any evolved star. Motivated by the detection of BN, we have performed a spectral line survey of TMC-1 to investigate its inventory of aromatic molecules.

Most interstellar molecules (>80%) have been discovered using pure rotational spectroscopy at radio frequencies (*3*). We therefore searched for PAHs using observations of TMC-1 in the range of 8 to 33.5 GHz, where rotational emission lines of many aromatic molecules are predicted to be strongest, given the 5 to 10 K temperature of this cloud (*4*). Using the 100-m Robert C. Byrd Green Bank Telescope (GBT), we initiated an observing project entitled GOTHAM (GBT Observations of TMC-1: Hunting Aromatic Molecules) to perform a spectral line survey of TMC-1. The first reduction of the GOTHAM data, comprising observations obtained between February 2018 and May 2019 (hereafter data release 1, or DR1), has near-continuous frequency coverage in the ranges of 8 to 11.6 GHz and 18 to 29.5 GHz, with a few small gaps. Details of these observations have been presented elsewhere (*4*, *5*). Further observations were obtained until June 2020 (hereafter DR2), which allowed us to extend the coverage to higher frequencies and improved the sensitivity in some regions already covered by DR1 (fig. S1) (*4*, *5*). Both datasets have a spectral resolution of 1.4 kHz, equivalent to a velocity resolution of 0.05 to 0.02 km s^{-1} (varying with frequency).

Given the previous detection of BN (*2*), a single benzene ring with an attached CN group, we searched for derivatives of naphthalene (two fused benzene rings; $C_{10}H_8$). Like benzene, naphthalene lacks a permanent dipole moment and therefore has no pure rotational spectrum. However, its CN-substituted derivatives, 1- and 2-cyanonaphthalene (1-CNN and 2-CNN; collectively CNNs), have large permanent dipole moments (Fig. 1) and laboratory-measured rotational spectra (*6*) that peak in the frequency region covered by our observations (fig. S3).

Similarly to BN (*2*), initial searches for the CNNs in our DR1 data showed no individual rotational lines above the noise level of the observations. We therefore calculated a spectral stack by combining the positions of all lines predicted in the dataset. Because the average excitation temperature of molecules (T_{ex} ~ 7 K) and the velocity (5.8 km s^{-1}) of TMC-1 are known from other species (*4*, *7*, *8*), we averaged the signal from all rotational transitions covered by our observations weighted by their predicted intensities and by the local noise level of the observations (*5*). The two

[1]Department of Chemistry, Massachusetts Institute of Technology, Cambridge, MA 02139, USA. [2]National Radio Astronomy Observatory, Charlottesville, VA 22903, USA. [3]Center for Astrophysics, Harvard & Smithsonian, Cambridge, MA 02138, USA. [4]Department of Physics and Astronomy, Benedictine College, Atchison, KS 66002, USA. [5]Center for Astrochemical Studies, Max Planck Institute for Extraterrestrial Physics, Garching, Germany. [6]Institute for Theoretical Chemistry, University of Stuttgart, Stuttgart, Germany. [7]Astrochemistry Laboratory and the Goddard Center for Astrobiology, NASA Goddard Space Flight Center, Greenbelt, MD 20771, USA. [8]Université de Rennes, Centre National de la Recherche Scientifique, Institut de Physique de Rennes, Unité Mixte de Recherche 6251, F-35000 Rennes, France. [9]Institute for Astrophysics and Computational Sciences, Department of Physics, Catholic University of America, Washington, DC 20064, USA. [10]Department of Chemistry, University of Virginia, Charlottesville, VA 22904, USA. [11]Department of Astronomy, University of Virginia, Charlottesville, VA 22904, USA. [12]Astro Space Center, Lebedev Physical Institute, Russian Academy of Sciences, Moscow, Russia.
*Corresponding author. Email: brettmc@mit.edu
†These authors contributed equally to this work.

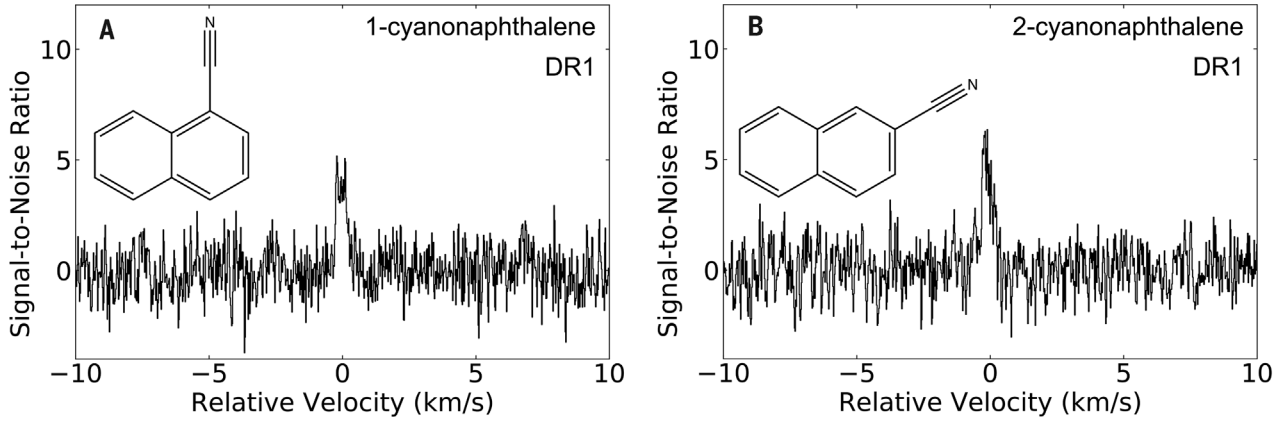

Fig. 1. Molecular structures and spectral stacks of 1-CNN and 2-CNN in the GOTHAM DR1 data. These molecules are derivatives of naphthalene, substituting a nitrile (–CN) group for a hydrogen atom. This substitution produces two distinct isomers, both of which are highly polar, with dipole moments (μ) along the *a* and *b* principal axes: (**A**) 1-CNN: μ_a = 3.6 debye, μ_b = 3.0 debye and (**B**) 2-CNN: μ_a = 5.1 debye, μ_b = 1.0 debye (*6*). The spectral stacks are shown relative to the TMC-1 systemic velocity of 5.8 km s^{-1}. The weighting process assumed an excitation temperature of T_{ex} = 7 K.

stacks for 1-CNN and 2-CNN derived from the DR1 data are shown in Fig. 1 and indicate the presence of both molecules.

We used the higher-quality DR2 dataset to determine the physical parameters [T_{ex}, column density (N_T), linewidth (ΔV), source size (θ), and velocity in the local standard of rest (v_{lsr})] that best reproduce the observations. A Markov chain Monte Carlo (MCMC) analysis was used to derive the physical parameters that best reproduce the stacked emission, including radiative transfer corrections for optical depth (*9*), which provides more robust uncertainty estimates than a least-squares fit. For this more detailed analysis, we assumed four partially overlapping Doppler velocity components with v_{lsr} between 5.5 and 6.1 km s^{-1}, as seen in observations of other species (*10*, *11*), each with their own column density and source size (the latter is poorly constrained in our single-dish observations). A single excitation temperature T_{ex} and linewidth ΔV (*4*, *12*, *13*) are assumed to apply to all four velocity components. We used the physical parameters from the more strongly detected BN (table S4 and fig. S15) as Gaussian priors in this analysis.

The results from the MCMC analysis for 1-CNN (table S5 and fig. S16) and 2-CNN (table S6 and fig. S17) yield total column densities (the sum of all four velocity components) of $7.35^{+3.33}_{-4.63} \times 10^{11}$ cm^{-2} and $7.05^{+3.23}_{-4.50} \times 10^{11}$ cm^{-2}, respectively. At those column densities, we predict that roughly a dozen lines of 1-CNN, and none of 2-CNN, should be above the local noise level in parts of the DR2 data. Figure 2 shows the DR2 data along with simulated profiles of those lines; all others are predicted to be below the noise. There is evidence for at least five lines with peak signal-to-noise ratios (SNRs) >4σ and tentative evidence for several others. Although these individual lines are weak, they provide us with additional confidence in the results of the stacking process.

The information content of the entire spectrum can also be used to assess the presence or absence of each molecule, which has many weak transitions at or below the root mean square (RMS) noise level of the observations. We performed this test using spectral stacking combined with matched filtering (*5*, *13*). Although care must be taken with respect to interloping signals and the noise characteristics of the data, this approach increases the SNR, with the averaged spectrum encapsulating the total information content of all observed lines, rather than examining each (lower-significance) line individually.

The details of this methodology, including analysis of the robustness, are presented elsewhere (*5*, *13*). Briefly, we extracted a small portion of the observations centered on the predicted frequency of each spectral line, discarding any windows with a spectral feature >5σ to avoid interloping signals from other species. A signal-to-noise weighted average of the spectra was then calculated on the basis of the expected intensity of the line (derived from the MCMC parameters) and the RMS noise of the observations, verified to contain no red-noise contamination (fig. S11). The results are shown in Fig. 3, A and C. Calculating the overall significance of any detections required us to consider the peak SNR in the central channel as well as the SNR of all channels that contain molecular emission. To do this, the model spectra were stacked using the same weights as those used for the observations, and the stacked model was then used as

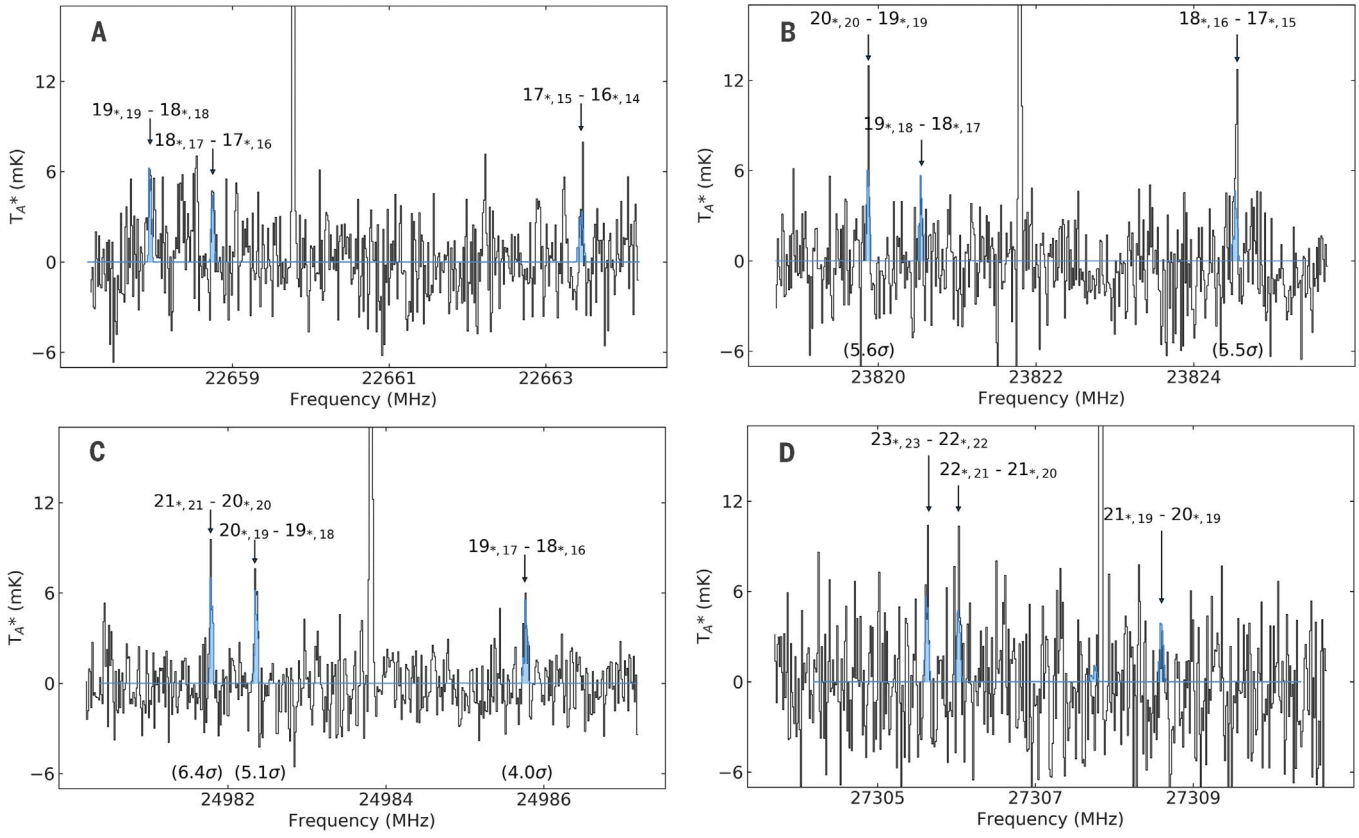

Fig. 2. GOTHAM DR2 spectra in the vicinity of the strongest predicted 1-CNN transitions. (**A** to **D**) Observations are shown in black, with simulated spectra of 1-CNN using the parameters derived from our MCMC analysis (table S5) overlaid in blue. The *y* axis is the atmosphere-corrected antenna temperature scale (T_A*). The observations have not been adjusted for the systemic velocity of TMC-1 (5.8 km s^{-1}). The spectra have been smoothed with a Hanning window to a resolution of 14 kHz for display. The quantum numbers of the transitions, ignoring hyperfine structure, are labeled at the predicted position of each line (arrows). Multiple closely spaced *K*-components of each transition contribute to each line and are denoted by asterisks. Transitions with SNRs ≥4σ are labeled in parentheses beneath the spectra.

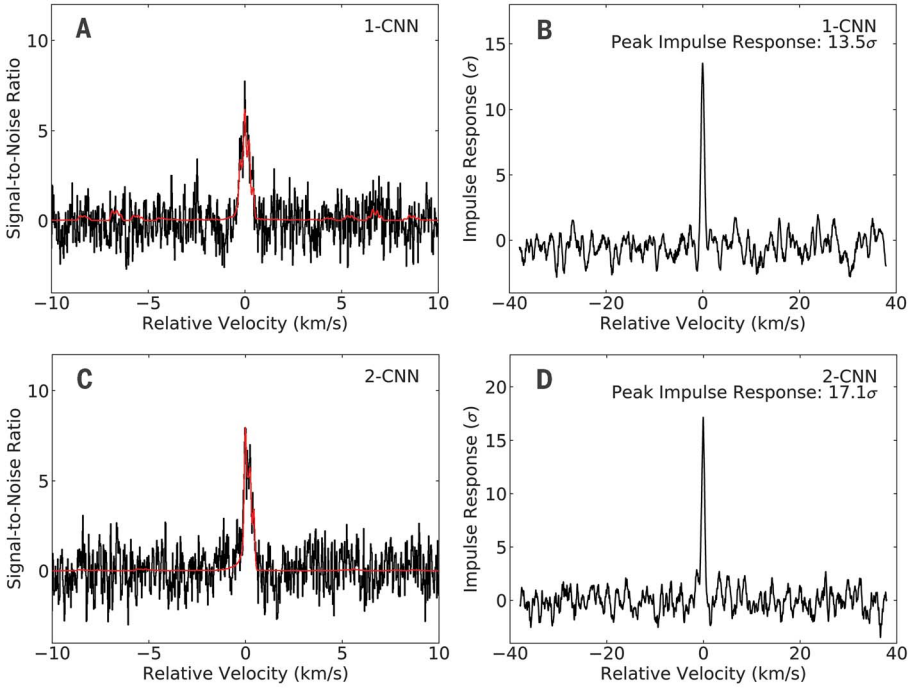

Fig. 3. Stacked spectra and impulse responses for the matched filtering analyses of 1-CNN and 2-CNN. The stacked spectra of (**A**) 1-CNN and (**C**) 2-CNN from the GOTHAM DR2 data are shown in black, overlaid with the line profile in red from the MCMC analysis of the DR2 data. The SNR is shown on a per-channel basis. Impulse response functions of the stacked spectra of (**B**) 1-CNN and (**D**) 2-CNN are shown, using the simulated line profiles as matched filters. The peak of the impulse response functions provides a minimum significance for the detections of 13.5σ and 17.1σ, respectively.

a matched filter that was cross-correlated with the stacked observations. The resulting impulse response spectrum provides a lower limit on the statistical significance (Fig. 3, B and D): 13.5σ for 1-CNN and 17.1σ for 2-CNN. We performed additional tests (*5*), including jack-knife tests (fig. S4) and checks for spurious detections (figs. S5 to S8 and S10), to evaluate the robustness of this methodology.

We conclude that both CNNs are detected in TMC-1. The presence of these PAH molecules in the interstellar medium (ISM) supports the hypothesis that PAHs are responsible for the unidentified infrared (UIR) emission bands (*1*). The UIR bands are composed of features at mid-infrared wavelengths characteristic of C–C and C–H stretching and bending motions of aromatic molecules, consistent with PAHs. Although the infrared spectra of different PAH molecules are readily distinguishable in the laboratory at high spectral resolution (*14*), the assignment of individual PAHs as carriers of the UIR features has not been possible because the differences in frequency are smaller than the width of the observed interstellar band profiles. It is therefore likely that many different PAHs contribute to the UIR emission bands (*1*). Although the carriers of the UIRs must have substantial aromatic character and PAHs are likely responsible for a sizable fraction of the overall emission, the specific structures and elemental compositions of the carriers remain a subject of debate (*15*). This uncertainty has limited the detailed analysis of sources that emit UIR bands (*16*).

We now consider the interstellar formation and destruction chemistry of 1-CNN and 2-CNN as individual molecules rather than PAHs in aggregate. Two scenarios have been proposed to explain the formation of PAHs: "top-down" and "bottom-up" formation chemistry. In the top-down scenario, small interstellar carbon clusters, or carbon soot particles in the envelopes of evolved stars, are broken down by ultraviolet (UV) radiation to form a variety of PAHs (*17*). PAHs may also be formed on the surfaces of interstellar dust grains in the envelopes of evolved stars (*18*). These PAHs are then distributed into the ISM, including molecular clouds. In the bottom-up scenario, PAHs are built in situ in molecular clouds from smaller precursors through chemical evolutionary pathways such as gas-phase ion-molecule and neutral-neutral reactions or reactions occurring on grain surfaces (*19*, *20*).

Any population of PAHs inherited by TMC-1 from prior top-down formation must have survived in the diffuse ISM. However, PAHs composed of less than ~20 to 30 atoms cannot radiatively stabilize upon absorption of a UV photon and are therefore destroyed in the diffuse ISM (*21*). The presence of small PAHs (CNNs) in TMC-1 suggests that at least some in situ bottom-up formation has occurred.

Existing astrochemical reaction networks do not include detailed PAH formation and destruction chemistry (*22*, *23*). We have extended a gas-grain chemical network (*24*) to include reactions relevant to naphthalene, 1-CNN, and 2-CNN, along with reactions relevant to other detections from the GOTHAM survey (*4*, *12*, *13*, *25*).

We included two major formation routes for naphthalene. The first is formation of $C_{10}H_8$, directly from the reaction of a phenyl radical with vinylacetylene

$$C_6H_5 + CH_2CHC_2H \rightarrow C_{10}H_8 + H \quad (R1)$$

This barrierless gas-phase reaction is viable under TMC-1–like conditions (*26*). The second route involves a dihydronaphthalene ($C_{10}H_{10}$) precursor that forms via the reaction between a phenyl radical and 1,3-butadiene

$$C_6H_5 + CH_2CHCHCH_2 \rightarrow C_{10}H_{10} + H \quad (R2)$$

This reaction is also expected to occur in the ISM (*27*). Successive abstraction of two hydrogen atoms from $C_{10}H_{10}$, both of which have no energy barrier (*28*), yields $C_{10}H_8$. For all species added to our network, we assume gas-phase depletion via both destructive reaction with ions (with rate coefficients calculated using the Langevin formula) and adsorption onto grains.

For 1-CNN and 2-CNN, we added the formation routes

$$C_{10}H_8 + CN \rightarrow \text{1-CNN} + H \quad (R3)$$

$$C_{10}H_8 + CN \rightarrow \text{2-CNN} + H \quad (R4)$$

assuming equal branching fractions. We assume that reactions R3 and R4 occur on every collision, because analogous reactions between CN radicals and unsaturated hydrocarbons such as benzene are known to be both barrierless and exothermic (*29*). We included a process for 1-CNN that is analogous to the one for naphthalene (*26*): This process involves the reaction of phenyl radicals (C_6H_5) with cyanovinylacetylene ($HC_2CHCHCN$), which presumably occurs at the collisional rate. However, we find that the contribution of this reaction to the 1-CNN abundance is small. Our reaction network operates with the assumption that the chemistry of PAHs in molecular clouds such as TMC-1 is predominantly in the gas phase, because the rate of thermal desorption of CNN from dust grains at ~10 K is negligible. Nonthermal desorption mechanisms may

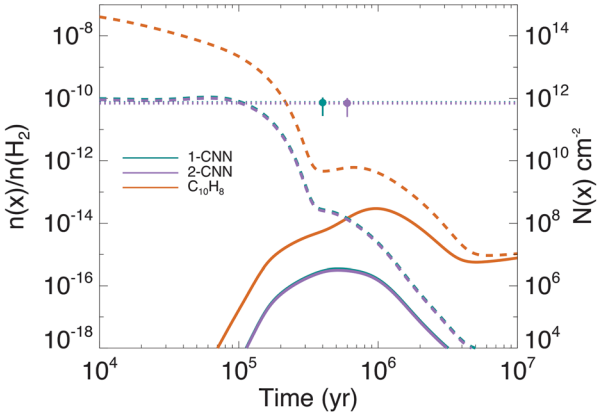

Fig. 4. Results of the astrochemical models. Calculated abundances of naphthalene (orange), 1-CNN (purple), and 2-CNN (teal) under TMC-1 conditions. Data for 1-CNN and 2-CNN overlap. Results are shown for our fiducial model (solid lines) and a model that assumes an initial naphthalene abundance of $n(C_{10}H_8)/n(H_2) = 1.0 \times 10^{-7}$ [where $n(x)$ is the volume density of molecule x] (dashed lines). The right y axis shows equivalent column densities, assuming $n(H_2) = 10^{22}$ cm^{-2}. The circles indicate the values for these species derived from our DR2 observations, with 1σ error bars, at arbitrary times. The dotted horizontal lines show these values extended over the range of the x axis for display.

allow for the introduction of aromatic molecules into the gas from icy surfaces (*30*) but are not included in our calculations.

The results of our simulations are shown in Fig. 4. In the fiducial model, the abundances of both 1- and 2-CNN are underpredicted by ≳6 orders of magnitude. CN is abundant in the model, so naphthalene is the limiting reagent. The large disparity between observations and predictions suggests that (i) additional production pathways for naphthalene may be missing, (ii) the efficiency of existing pathways is substantially underestimated, or (iii) a nontrivial initial abundance of naphthalene is inherited from prior top-down chemistry. To test scenario (iii), we performed a second calculation to ascertain how PAHs inherited from earlier stages of cloud evolution affect the abundances of 1- and 2-CNN under TMC-1 conditions. For this model, we added an initial abundance of naphthalene (representing an inherited population) tuned to reproduce the observational data. We found agreement with the observations for a naphthalene abundance of $n(C_{10}H_8)/n(H_2) = 1.0 \times 10^{-7}$ at early times, where n refers to the volume density. This would correspond to ~1% of the total carbon. However, the calculated abundances of 1-CNN and 2-CNN again deviate from the observational values at times $>10^5$ years, the typical lifetime of sources such as TMC-1.

Our calculations neglect grain-surface formation pathways (*5*). Nevertheless, we regard the required initial abundance of naphthalene as unrealistically large, which in turn implies that a purely top-down formation pathway is also disfavored. Conversely, the pathways we have considered for in situ bottom-up formation are also insufficient to reproduce observations. Other pathways are required, such as ion-neutral reactions. Such processes are generally efficient under interstellar conditions and can lead to $C_{10}H_9^+$ (*31*), which may form naphthalene as a product of its dissociative recombination with electrons in a manner analogous to the benzene formation route from $C_6H_7^+$ (*32*).

We conclude that two PAHs—1-CNN and 2-CNN—are present in the molecular cloud TMC-1. We are unable to explain the derived abundances with either top-down or bottom-up formation scenarios, indicating that other routes may be required or that existing routes may be more efficient than previously thought.

REFERENCES AND NOTES

1. A. G. G. M. Tielens, *Annu. Rev. Astron. Astrophys.* **46**, 289–337 (2008).
2. B. A. McGuire *et al.*, *Science* **359**, 202–205 (2018).
3. B. A. McGuire, *Astrophys. J. Suppl. Ser.* **239**, 17 (2018).
4. B. A. McGuire *et al.*, *Astrophys. J.* **900**, L10 (2020).
5. Materials and methods are available as supplementary materials.
6. D. McNaughton *et al.*, *Mon. Not. R. Astron. Soc.* **476**, 5268–5273 (2018).
7. P. Gratier *et al.*, *Astrophys. J. Suppl. Ser.* **225**, 25 (2016).
8. N. Kaifu *et al.*, *Publ. Astron. Soc. Jpn.* **56**, 69–173 (2004).
9. B. E. Turner, *Astrophys. J. Suppl. Ser.* **76**, 617 (1991).
10. K. Dobashi *et al.*, *Astrophys. J.* **864**, 82 (2018).
11. K. Dobashi *et al.*, *Astrophys. J.* **879**, 88 (2019).
12. C. Xue *et al.*, *Astrophys. J.* **900**, L9 (2020).
13. R. A. Loomis *et al.*, *Nat. Astron.* **5**, 188–196 (2021).
14. D. M. Hudgins, S. A. Sandford, *J. Phys. Chem. A* **102**, 329–343 (1998).
15. S. Kwok, Y. Zhang, *Nature* **479**, 80–83 (2011).
16. C. W. Bauschlicher Jr., A. Ricca, C. Boersma, L. J. Allamandola, *Astrophys. J. Suppl. Ser.* **234**, 32 (2018).
17. O. Berné, J. Montillaud, C. Joblin, *Astron. Astrophys.* **577**, A133 (2015).
18. L. Martínez *et al.*, *Nat. Astron.* **4**, 97–105 (2020).
19. P. M. Woods, T. J. Millar, A. A. Zijlstra, E. Herbst, *Astrophys. J.* **574**, L167–L170 (2002).
20. B. M. Jones *et al.*, *Proc. Natl. Acad. Sci. U.S.A.* **108**, 452–457 (2011).
21. M. Chabot, K. Béroff, E. Dartois, T. Pino, M. Godard, *Astrophys. J.* **888**, 17 (2020).
22. R. P. A. Bettens, E. Herbst, *Astrophys. J.* **468**, 686 (1996).
23. R. Bettens, E. Herbst, *Astrophys. J.* **478**, 585–593 (1997).
24. C. N. Shingledecker, J. Tennis, R. L. Gal, E. Herbst, *Astrophys. J.* **861**, 20 (2018).
25. M. C. McCarthy *et al.*, *Nat. Astron.* **5**, 176–180 (2020).
26. D. S. N. Parker *et al.*, *Proc. Natl. Acad. Sci. U.S.A.* **109**, 53–58 (2012).
27. R. I. Kaiser *et al.*, *J. Phys. Chem. A* **116**, 4248–4258 (2012).
28. P. A. Jensen *et al.*, *Mon. Not. R. Astron. Soc.* **486**, 5492–5498 (2019).
29. I. R. Cooke, D. Gupta, J. P. Messinger, I. R. Sims, *Astrophys. J.* **891**, L41 (2020).
30. D. Marchione, J. D. Thrower, M. R. S. McCoustra, *Phys. Chem. Chem. Phys.* **18**, 4026–4034 (2016).
31. V. G. Anicich, "An index of the literature for bimolecular gas phase cation-molecule reaction kinetics" (JPL Publication 03-19, NASA, 2003); http://hdl.handle.net/2014/7981.
32. M. J. McEwan *et al.*, *Astrophys. J.* **513**, 287–293 (1999).
33. GOTHAM Collaboration, Spectral Stacking Data for Phase 2 Science Release of GOTHAM, Version 3.0, Harvard Dataverse (2020); https://doi.org/10.7910/DVN/K9HRCK.
34. GOTHAM Collaboration, Replication Data for Astrochemical Models in the Detection of 1- and 2-cyanonaphthalene, Version 2.0, Harvard Dataverse (2021); https://doi.org/10.7910/DVN/OMYNAE.

ACKNOWLEDGMENTS

The National Radio Astronomy Observatory is a facility of the National Science Foundation (NSF) operated under cooperative agreement by Associated Universities, Inc. The Green Bank Observatory is a facility of the NSF operated under cooperative agreement by Associated Universities, Inc. **Funding:** B.A.M. was supported by NASA through Hubble Fellowship grant HST-HF2-51396 awarded by the Space Telescope Science Institute, which is operated by the Association of Universities for Research in Astronomy, Inc., for NASA, under contract NAS5-26555. A.M.B. acknowledges support from the Smithsonian Institution as a Submillimeter Array (SMA) Fellow. M.C.M. and K.L.K.L. acknowledge financial support from NSF grants AST-1908576 and AST-1615847 and NASA grant 80NSSC18K0396. C.N.S. thanks the Alexander von Humboldt Stiftung/Foundation for their generous support, as well as V. Wakelam for use of the NAUTILUS v1.1 code. I.R.C. acknowledges funding from the European Union's Horizon 2020 research and innovation program under the Marie Skłodowska-Curie grant agreement 845165-MIRAGE. S.B.C. and M.A.C. were supported by the NASA Astrobiology Institute through the Goddard Center for Astrobiology. E.H. thanks the NSF for support through grant AST 1906489. C.X. is a Grote Reber Fellow, and support for this work was provided by the NSF through the Grote Reber Fellowship Program administered by Associated Universities, Inc./National Radio Astronomy Observatory and the Virginia Space Grant Consortium. **Author contributions:** Conceptualization: B.A.M., A.M.B., A.J.R., and S.K.; Methodology: B.A.M., A.M.B., K.L.K.L., and R.A.L.; Software: R.A.L., K.L.K.L., and B.A.M.; Data curation: B.A.M., R.A.L., A.M.B., K.L.K.L., C.X., M.A.S., A.J.R., and I.R.C.; Modeling: C.N.S., A.M.B., C.X., E.R.W., S.B.C., and E.H.; Writing – original draft: B.A.M., A.M.B., R.A.L., C.N.S., K.L.K.L., and M.C.M.; Writing – review & editing: all authors. **Competing interests:** We declare no competing interests. **Data and materials availability:** All of our GBT and VLA data are available in the NRAO archive at https://archive.nrao.edu/archive/advquery.jsp under project codes AGBT17A_164, AGBT17A_434, AGBT18A_333, AGBT18B_007, AGBT19A_047, and TCAL0003. Observational data windowed around these transitions; the full catalogs, including spectroscopic properties of each transition; and the partition function used in the MCMC analysis are available in the Harvard Dataverse repository (*33*). We obtained the NAUTILUS code from http://perso.astrophy.u-bordeaux.fr/~vwakelam/Nautilus.html. Input and output files for the astrochemical models are also available in Harvard Dataverse (*34*).

SUPPLEMENTARY MATERIALS

science.sciencemag.org/content/371/6535/1265/suppl/DC1
Materials and Methods
Supplementary Text
Figs. S1 to S19
Tables S1 to S6
References (*35*–*59*)

16 March 2020; accepted 4 February 2021
10.1126/science.abb7535

Detection of two interstellar polycyclic aromatic hydrocarbons via spectral matched filtering

Brett A. McGuire, Ryan A. Loomis, Andrew M. Burkhardt, Kin Long Kelvin Lee, Christopher N. Shingledecker, Steven B. Charnley, Ilsa R. Cooke, Martin A. Cordiner, Eric Herbst, Sergei Kalenskii, Mark A. Siebert, Eric R. Willis, Ci Xue, Anthony J. Remijan and Michael C. McCarthy

Science **371** (6535), 1265-1269.
DOI: 10.1126/science.abb7535

Identifying PAHs in space

Midinfrared spectroscopy has shown that polycyclic aromatic hydrocarbons (PAHs) are abundant in many astronomical objects, but this technique cannot determine which specific PAH molecules are present. Radio astronomy could provide individual identifications if the molecule is sufficiently abundant and has a large dipole moment, but PAHs are expected to produce large numbers of very weak lines. McGuire *et al.* performed a stacking and matched filter analysis to search for PAHs in radio observations of TMC-1, located within the interstellar Taurus Molecular Cloud. They identified emission from two isomers of the small PAH cyanonapthalene, two fused benzene rings with a CN group attached.

Science, this issue p. 1265